Available online at www.sciencedirect.com
ScienceDirect
Journal of Power Sources 158 (2006) 1463–1471
JOURNAL OF POWER SOURCES
www.elsevier.com/locate/jpowsour

Effects of Pd substitution on the electrochemical properties of $Mg_{0.9-x}Ti_{0.1}Pd_xNi$ ($x = 0.04$–0.1) hydrogen storage alloys

Qi-Feng Tian [a,b], Yao Zhang [a,b,*], Li-Xian Sun [a,b,*], Fen Xu [a,b], Zhi-Cheng Tan [a,b], Hua-Tang Yuan [c], Tao Zhang [a,b]

[a] *Dalian Institute of Chemical Physics, Chinese Academy of Sciences, Dalian 116023, China*
[b] *Graduate School of the Chinese Academy of Sciences, Beijing 100049, China*
[c] *Institute of New Energy Material Chemistry, Nankai University, Tianjin 300071, China*

Received 5 August 2005; received in revised form 14 October 2005; accepted 17 October 2005
Available online 28 November 2005

Abstract

Amorphous $Mg_{0.9-x}Ti_{0.1}Pd_xNi$ ($x = 0.04$–0.1) hydrogen storage alloys were prepared by mechanical alloying (MA). The effects of Pd substitution on the electrochemical properties of the $Mg_{0.9-x}Ti_{0.1}Pd_xNi$ ($x = 0.04$–0.1) electrode alloys were studied by cyclic charge–discharge, linear polarization, anodic polarization, electrochemical impedance spectroscopy (EIS), and hydrogen diffusion coefficient experiments. It was found that the cyclic capacity retention rate C_{50}/C_1 of the quaternary alloys was greatly improved due to the substitution of Pd for Mg. $Mg_{0.8}Ti_{0.1}Pd_{0.1}Ni$ electrode alloy retained the discharge capacity above 200 mAh g^{-1} even after 80 charge–discharge cycles, possessing the longest cycle life in the studied quaternary alloys. The improvement of cycle life was ascribed to the formation of passive film on the surface of these electrode alloys. X-ray photoelectron spectroscopy (XPS) analysis proved that the passive film was composed of $Mg(OH)_2$, TiO_2, NiO, and PdO, which synergistically protected the alloy from further oxidation. The Auger Electron Spectroscopy (AES) study revealed that the thickness of passive film increased with augmentation of the Pd content. The electrochemical impedance study of electrode alloys after different cycles demonstrated that the passive film became thicker during cycles and its thickness also increased with Pd content augmentation. It was also found that the augmentation of Pd content resulted in the decrease of exchange current density I_0 and the increase of the charge-transfer resistance R_{ct}. With increasing the Pd amount in the $Mg_{0.9-x}Ti_{0.1}Pd_xNi$ ($x = 0.04$–0.1) electrode alloys, hydrogen diffusion coefficient D was gradually enhanced at first. Then, it decreased with augmentation of cycle due to the growth of passive film on the surface of the alloys.

Keywords: Mg-based electrode alloys; Hydrogen storage; Mechanical alloying; Electrochemical properties; Substitutions

1. Introduction

MgNi amorphous hydrogen storage alloys are considered as a promising candidate for the cathode material of Ni-MH batteries because of its large discharge capacity [1], light weight, and low cost. Unfortunately, its cycle life is too short to meet the need of applications. It is clear that Mg is easily oxidized in the KOH solution and its discharge capacity declines very quickly.

Many efforts such as element substitution on both Mg and Ni sides have been tried to inhibit the corrosion of Mg and improve the cyclic discharge stability of MgNi electrode alloys [2,3]. Recently the partial substitution of Ti for Mg in MgNi alloys attracted more attentions [4–7]. It was found that the Ti substitution inhibited the capacity degradation effectively. The cycle life of the $Mg_{1-x}Ti_xNi$ ($x = 0.1$, 0.2, and 0.3) electrode alloys was prolonged to more than 20 cycles above 200 mAh g^{-1}. However, the present cyclic stability of Mg–Ti–Ni alloys still cannot meet the real requirements of Ni-MH batteries. Therefore, the element substitution will be further investigated on the basis of the Mg–Ti–Ni alloys in this work.

Pd was found possessing higher electrocatalytic activity than Ni for the hydrogen evolution reaction (HER) in the electrochemical cycle [8]. It is beneficial to improving not only the charge–discharge activities of Mg-based electrode alloys [9,10], but also the anti-corrosion properties [11,12] of those amorphous

* Corresponding authors. Tel.: +86 411 84379215; fax: +86 411 84379213.
E-mail addresses: zhangyao@dicp.ac.cn (Y. Zhang), lxsun@dicp.ac.cn (L.-X. Sun).

0378-7753/$ – see front matter © 2005 Elsevier B.V. All rights reserved.
doi:10.1016/j.jpowsour.2005.10.068

alloys. Park et al. [13] performed in situ Pd deposition on Mg_2Ni electrodes during the charge cycles, which was found enhancing the cyclic stability of the nano-crystalline Mg_2Ni electrode in the Pd-added electrolyte. Yamaura et al. also found that Pd addition can extend cycle life of Mg_2Ni-based alloys prepared by melt spun [14,15].

In our previous work [16], the electrochemical performances of $Mg_{0.9}Ti_{0.1}Ni_{1-x}Pd_x$ ($x = 0$–0.15) electrode alloys were intensively studied. The cyclic stability of the quaternary alloys was higher than that of $Mg_{0.9}Ti_{0.1}Ni$ alloy. However, the maximum discharge capacities decreased noticeably and yet the charge-transfer velocities declined slightly. Since the element Ni in MgNi-based alloys was of fundamental importance for both discharge capacity and charge-transfer kinetics, it could not be sacrificed in the present work. Therefore, Ni still kept the same atomic ratio as the $Mg_{0.9}Ti_{0.1}Ni$ when Mg was partially substituted by Pd in the quaternary alloys. The effects of Pd substitution on the electrochemical performances of the quaternary alloys will be discussed intensively in this paper.

2. Experimental

$Mg_{0.9-x}Ti_{0.1}Pd_xNi$ ($x = 0.04$–0.1) alloys were prepared by mechanically alloying (MA). The purity of all metal powders was higher than 99.5%. The powder mixtures as designed stoichiometry were ground by a planetary ball mill under Ar atmosphere for 120 h. In each milling pot, the ball to powder weight ratio was 30:1. The structure of the alloys was characterized by XRD (Rigaku D/max-2500, Cu Kα, 50 kV, 200 mA) and transmission electron microscopy (JEM-2000EX).

The tested electrodes for electrochemical experiments were fabricated by mixing 0.1 g alloy powder with 0.3 g electrolytic Cu powder. The mixture was then pressed into a pellet of 1.0 cm in diameter under a pressure of 30 MPa. Both sides of the pellet were coated with two foam nickel sheets, then pressed at 25 MPa and tightly spot-welded. A nickel lead wire was attached to this pressed foam nickel sheet by spot welding. The $NiOOH/Ni(OH)_2$ electrode and Hg/HgO electrode were used as counter and reference electrode, respectively. The electrolyte was 6 M KOH aqueous solution. Charge–discharge cycles of electrodes were conducted by an automatic LAND battery test instrument. The electrodes were charged for 3 h at a current density of 300 mA g^{-1}, rested for 5 min and then discharged to −0.6 V versus Hg/HgO electrode at a current density of 100 mA g^{-1}. All the measurements were carried out at the temperature of 303 K.

The linear polarization (LP) and anodic polarization (AP) curves of the electrodes were measured on Zahner Elektrik IM6e electrochemical workstation by scanning the electrode potential. The scanning rates were 0.1 mV s^{-1} from −5 to 5 mV (versus open circuit potential) for LP and 1 mV s^{-1} from 0 to 500 mV (versus open circuit potential) for AP at 50% depth of discharge (DOD) of the first cycle, respectively. The electrode kinetics parameters and the properties of passive film on the alloy surface were studied by electrochemical impedance spectroscopy (EIS) measurements. For the investigation of electrode kinetics parameters, the measurements were conducted from 5 mHz to 10 kHz with an amplitude of 5 mV versus open circuit potential at 50% DOD of the first cycle. The dependency of the growth of surface passive film upon cycle number was studied by the EIS with the above operational parameters at the end of the 9th, 20th, 32nd, and 40th cycle, respectively. To investigate the oxidation state of each metallic element on the surface, XPS detection were carried out on a PHI-550 type spectrometer at 10^{-8} Torr using Al Kα radiation. AES depth profiles detections were performed upon the same apparatus for revealing the elemental distribution on the particle surface of the alloys at the end of the 40th cycle with an electron beam at 10 kV and 30 mA. The electrode surface was sputtered with Ar^+ on an area of 1.5 mm × 1.5 mm at 4 kV and 15 mA.

The hydrogen diffusion coefficients were determined by potential step method, which were performed at the fully charged state of the 1st, 10th, 21st, 33rd, and 41st cycle, respectively. A +500 mV potential step was applied and the discharge time was 2500 s. Before tests, the particle radius of the $Mg_{0.9-x}Ti_{0.1}Pd_xNi$ ($x = 0.04$–0.1) alloy powders was ensured around 50 μm by sieving.

3. Results and discussion

3.1. The phase structure of the alloys

Fig. 1 shows the X-ray diffraction patterns for the $Mg_{0.9-x}Ti_{0.1}Pd_xNi$ ($x = 0.04$–0.1) quaternary alloys after 120 h ball milling. For each alloy, a broad Bragg peak was observed at approximately 42° (2θ). No secondary phase was detected in the patterns, which suggested that a single amorphous phase formed in these alloys after 120 h ball milling. TEM observations were performed in the present work for the further check. Fig. 2 is the selected area electron diffraction (SAED) image of $Mg_{0.8}Ti_{0.1}Pd_{0.1}Ni$ alloy. The ambiguous broad ring in SAED image demonstrated that the structure of the alloy was amorphous. The other quaternary alloys were also verified to possess

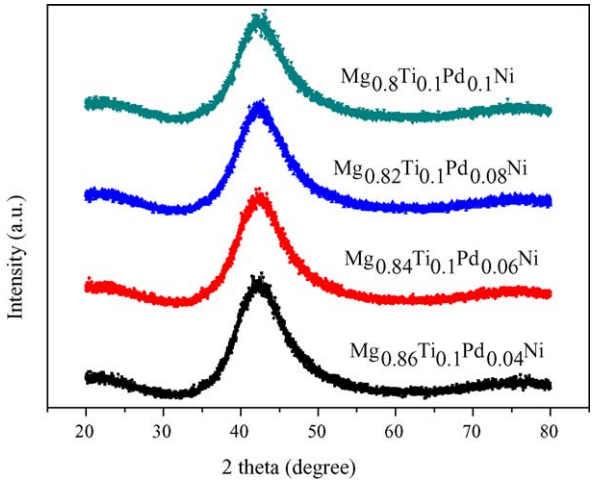

Fig. 1. XRD patterns of the $Mg_{0.9-x}Ti_{0.1}Pd_xNi$ ($x = 0.04$–0.1) alloy powders after mechanical alloying of 120 h.

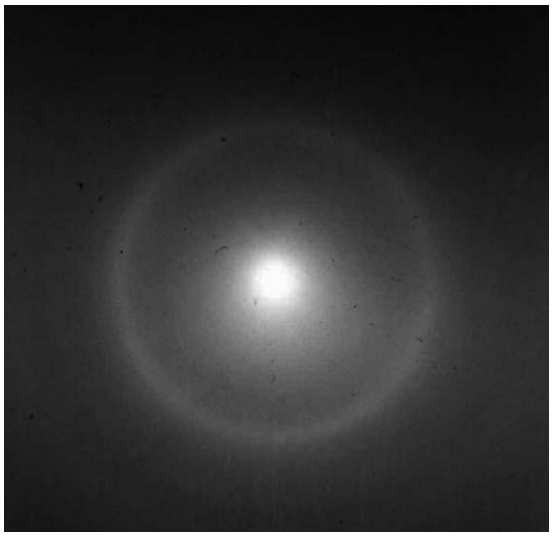

Fig. 2. The selected area electron diffraction image of the $Mg_{0.8}Ti_{0.1}Pd_{0.1}Ni$ alloy after ball milling of 120 h.

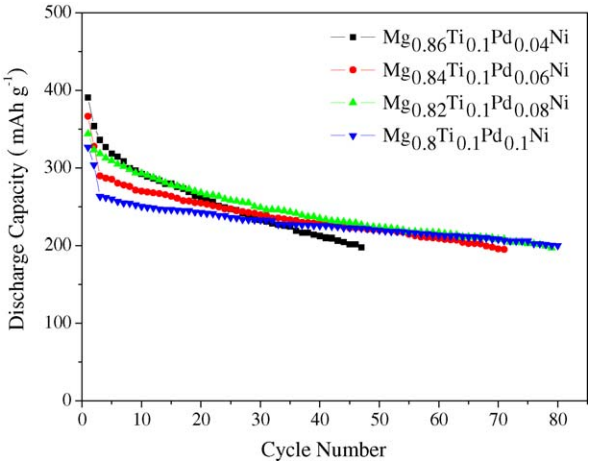

Fig. 3. The discharge capacity of the $Mg_{0.9-x}Ti_{0.1}Pd_xNi$ ($x = 0.04$–0.1) electrode alloys as a function of cycle number at 303 K.

the same structure as that of the $Mg_{0.8}Ti_{0.1}Pd_{0.1}Ni$ alloy by both XRD and TEM analyses.

3.2. Discharge capacity and cyclic stability

Fig. 3 exhibits the relationship between discharge capacities of $Mg_{0.9-x}Ti_{0.1}Pd_xNi$ ($x = 0.04$–0.1) electrode alloys and cycle number. For these alloys, the initial discharge capacities were usually the maximum capacities. It is obvious that the cyclic stability of the $Mg_{0.9-x}Ti_{0.1}Pd_xNi$ ($x = 0.04$–0.1) electrode alloys is much higher than that of the $Mg_{0.9}Ti_{0.1}Ni$ [4–7] by comparing their cyclic retention rate C_{20}/C_{max} and C_{50}/C_{max} (see Table 1). It is noted that the quaternary $Mg_{0.9-x}Ti_{0.1}Pd_xNi$ ($x = 0.04$–0.1) electrode alloys went through more charge–discharge cycles above 200 mAh g^{-1} than ternary Mg–Ti–Ni alloy. The $Mg_{0.8}Ti_{0.1}Pd_{0.1}Ni$ possessed the longest cycle life (more than 80 cycles above 200 mAh g^{-1}) among the studied alloys, which was also higher than most reported MgNi-based amorphous alloys as to the knowledge of the authors. The effect of Pd on the cycle life of the alloys agreed well with that obtained by Ma et al. [11,12], in which Pd was used to modify the surface and the bulk of the MgNi amorphous alloy. In this work, Pd dissolved completely in the amorphous phase of the $Mg_{0.9-x}Ti_{0.1}Pd_xNi$ ($x = 0.04$–0.1) alloys during the mechanical alloying. No residual Pd powder was found according to the XRD pattern in Fig. 1. It means that Pd dispersed homogeneously in the alloys and inhibited the corrosion from alkaline solution more effectively. It is possible for Pd to form combined passive films with Ti on the surface of the alloys particles and exert synergetic effects of corrosion inhibition as previously studied MgTiZrNi alloys [17,18].

The discharge capacities of the $Mg_{0.9-x}Ti_{0.1}Pd_xNi$ ($x = 0.04$–0.1) electrode alloys were larger than our previously studied $Mg_{0.9}Ti_{0.1}Ni_{1-x}Pd_x$ ($x = 0$–0.15) electrode alloys [16], although the Mg content in the former alloys was lower than that in the latter. It was suggested that the discharge capacity of the Mg–Ti–Pd–Ni alloys is more concerned with the content of Ni than Mg. Besides corrosion inhibition, Ni plays very important electrocatalytic role in the electrode process such as charge-transfer on the surface and hydrogen diffusion in the bulk of MgNi-based alloys. The oxidation of Ni might lead to the retardance of the electrode kinetics. The poor kinetics would also inhibit the discharge performance even though there are a lot of hydrogen absorbable elements like Mg and Pd in the alloys.

3.3. Passive films and its correlation with cycling stability

Fig. 4(a–e) are the O(1s), Mg(2p), Ni(2p), Pd(3d), and Ti(2p) XPS spectra of the outermost surface of the $Mg_{0.9-x}Ti_{0.1}Pd_xNi$ ($x = 0.04$–0.1) electrode alloys, after 40 charge–discharge cycles, respectively. The O(1s) spectra of these alloys show that the binding energy becomes lower with increasing Pd content. It indicated that the degree of oxidation on the alloy sur-

Table 1
The discharge capacities and cyclic stability of the $Mg_{0.9-x}Ti_{0.1}Pd_xNi$ ($x = 0.04$–0.1) and the $Mg_{0.9}Ti_{0.1}Ni$ electrode alloys

x	Maximum discharge capacity (mAh g^{-1})	Discharge capacity retention rate, C_{20}/C_1 (%)	Discharge capacity retention rate, C_{50}/C_1 (%)	The cycle number of the discharge capacity above 200 mAh g^{-1}
0	455	31.6	–	–
0.04	390.7	66.7	–	46
0.06	366.5	69.4	59.9	67
0.08	343.9	77.8	64.8	77
0.1	326.5	74.2	67.2	80

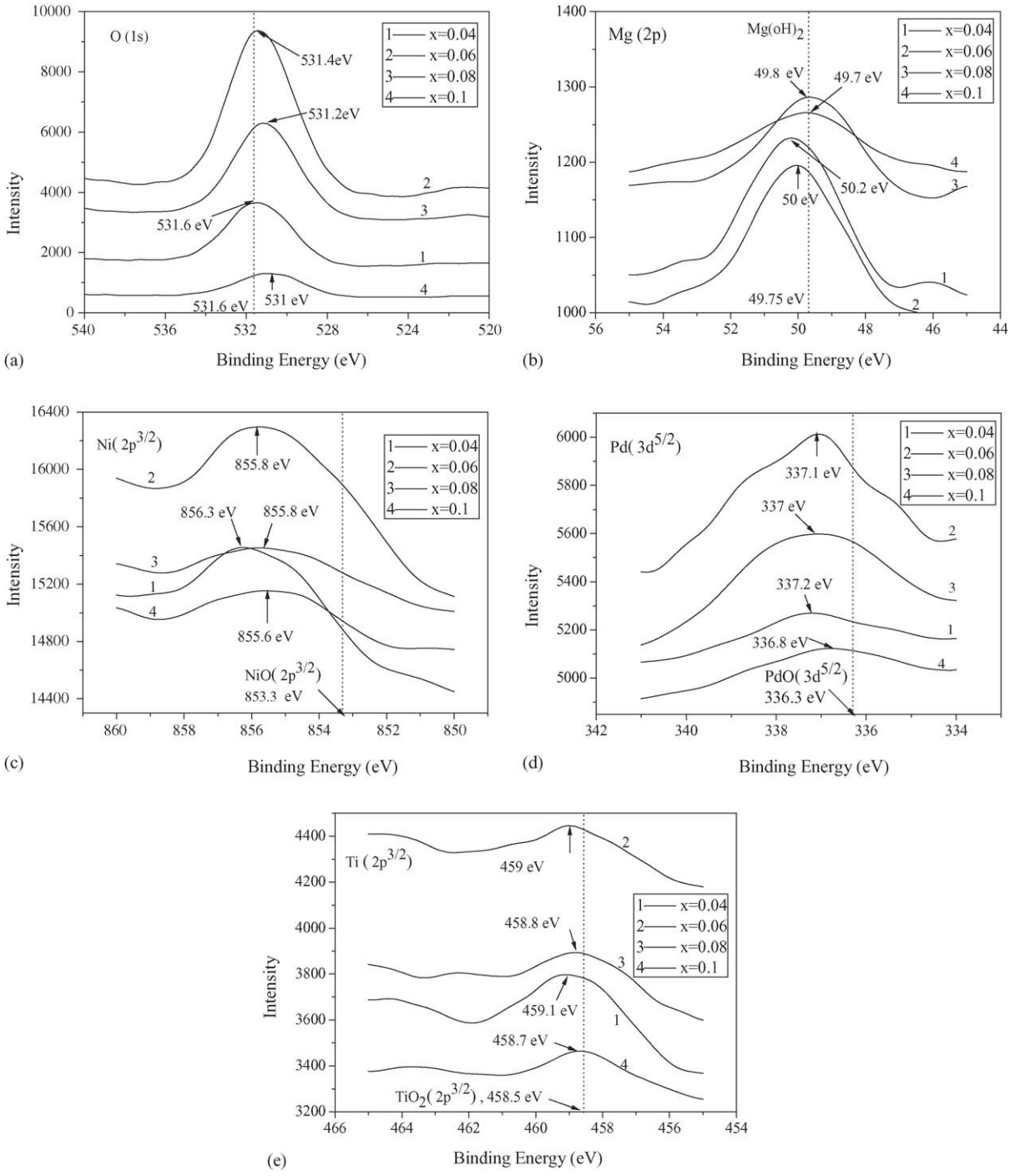

Fig. 4. The XPS spectra of the $Mg_{0.9-x}Ti_{0.1}Pd_xNi$ ($x = 0.04$–0.1) electrode alloys after 40 charge–discharge cycles: (a) O(1s); (b) Mg(2p); (c) Ni(2p); (d) Pd(3d); (e) Ti(2p).

face was weakened as Pd content increased. A similar tendency was observed for the spectra of Mg(2p) in Fig. 4(b). The increase of Pd content decreased the binding energy of Mg(2p), which means that the introduction of Pd suppressed effectively the oxidation of Mg on the surface of the alloys. From Fig. 4(c–e), it can also be seen that Ni, Pd, and Ti on the surface of the $Mg_{0.9-x}Ti_{0.1}Pd_xNi$ ($x = 0.04$–0.1) electrode alloys are transformed to NiO, PdO, and TiO_2, respectively in the 6 M KOH solution. Since these metallic oxides are insoluble and compact in alkaline aqueous solution, we believed that they formed a more corrosion-resistant passive oxide composite $(NiO)_x(PdO)_y(TiO_2)_z$ interspersed in the porous $Mg(OH)_2$ passive film. This passive film made the penetration of OH^- ion more difficult and protected the inner fresh alloy from being oxidized more effectively.

The impedance spectroscopy data were obtained at the end of the 9th, 20th, 32nd, and 40th cycle, respectively. Fig. 5 exhibits the impedance-phase angle plots of $Mg_{0.9-x}Ti_{0.1}Pd_xNi$

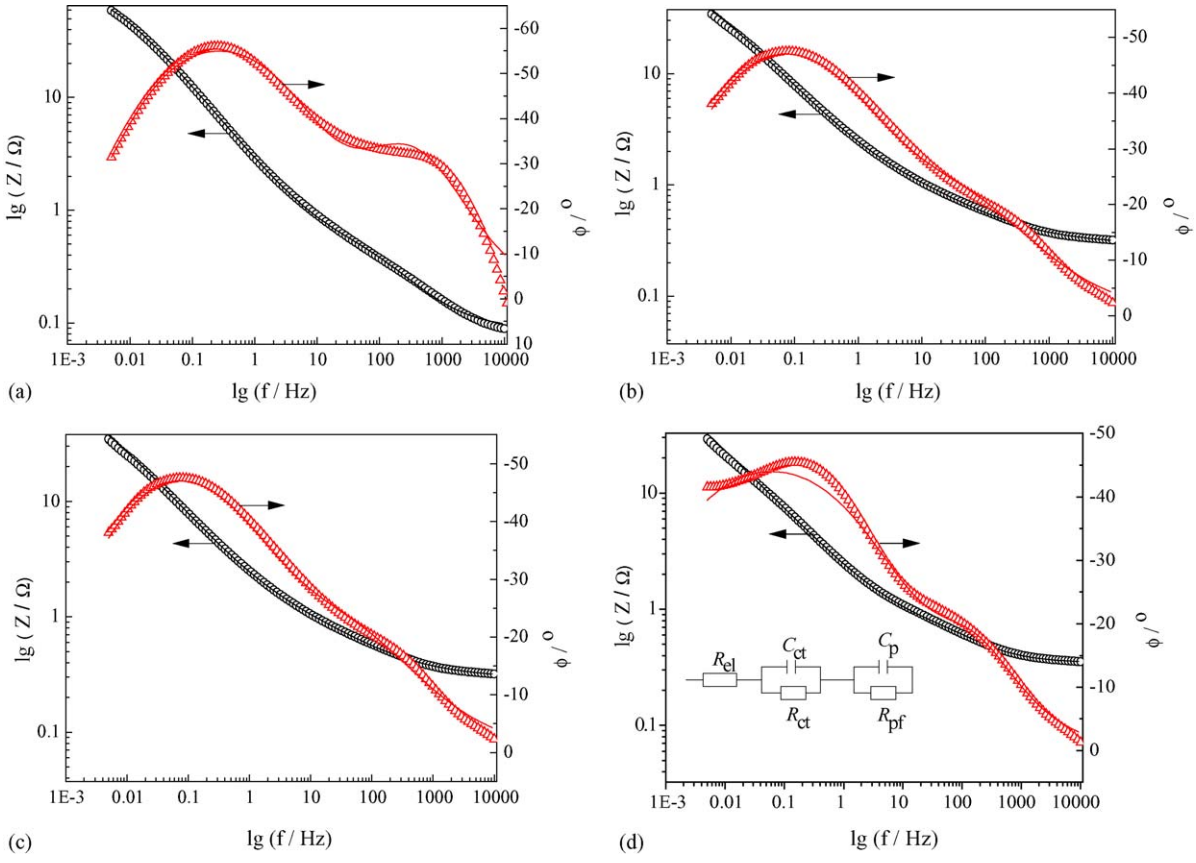

Fig. 5. The Bode plots of the $Mg_{0.9-x}Ti_{0.1}Pd_xNi$ ($x = 0.04$–0.1) electrode alloys at the end of 20th cycle: (a) $Mg_{0.86}Ti_{0.1}Pd_{0.04}Ni$; (b) $Mg_{0.84}Ti_{0.1}Pd_{0.06}Ni$; (c) $Mg_{0.82}Ti_{0.1}Pd_{0.08}Ni$; (d) $Mg_{0.8}Ti_{0.1}Pd_{0.1}Ni$ (◯: measured impedance; △: measured phase angle: —, simulated value).

($x = 0.04$–0.1) electrode alloys at the end of 20th cycle. The Bode plots of the studied alloys showed two maxima of phase angle, which reflected the presence of two time constants denoting the electrode process. The impedance data were analyzed with the proposed equivalent circuit as shown in the inset of Fig. 5(d). In the figure, the capacitive components labeled by C are modeled as constant-phase elements (CPE) to describe the depressed nature of the semicircles. R_{el} denotes the electrolyte resistance between the MH electrode and the reference electrode. R_{ct} and C_{ct}, representing the semicircle in the low-frequency region contribute to the charge-transfer reaction resistance and the double-layer capacitance, respectively. The passive film resistance and capacitance on the surface of the alloy particles generate the parameters R_{pf} and C_{pf}, respectively. It was concluded that the proposed equivalent circuit fitted well with the present system as seen in Fig. 5. It was also found that the reciprocal of C_{pf} value increased with the augmentation of cycle number from Fig. 6. Since the value of $1/C_{pf}$ is usually proportional to the thickness of passive film according to Badawy et al. [19], one can conclude that the thickness of passive film increased with the augmentation of cycle number. In addition, it can also be deduced from Fig. 6 that the higher Pd content in the alloys, the thicker of the passive film formed on the particle surface. It means that Pd is beneficial to the growth of passive film on the surface. The increment of the film thickness of the alloys with higher Pd content ($x = 0.08$ and 0.1) is larger than that containing lower Pd content ($x = 0.04$ and 0.06). Therefore, both Pd content and cycle number determined the thickness of passive film. The growth of passive film is consistent with the improvement of the cycle stability of studied electrode alloys.

Fig. 7(a–d) shows the AES depth profiles of the chief elements in the $Mg_{0.9-x}Ti_{0.1}Pd_xNi$ ($x = 0.04$–0.1) electrode alloys after 40 charge–discharge cycles. It was found that within the same sputter time or depth, the oxygen content dropped drastically for the $Mg_{0.8}Ti_{0.1}Pd_{0.1}Ni$ alloy, but more gradually for

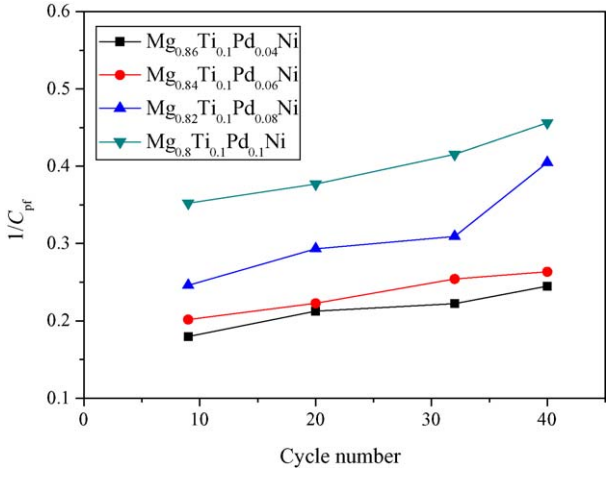

Fig. 6. The variation of $1/C_{pf}$ vs. cycle number for the $Mg_{0.9-x}Ti_{0.1}Pd_xNi$ ($x = 0.04$–0.1) electrode alloys during charge–discharge cycles.

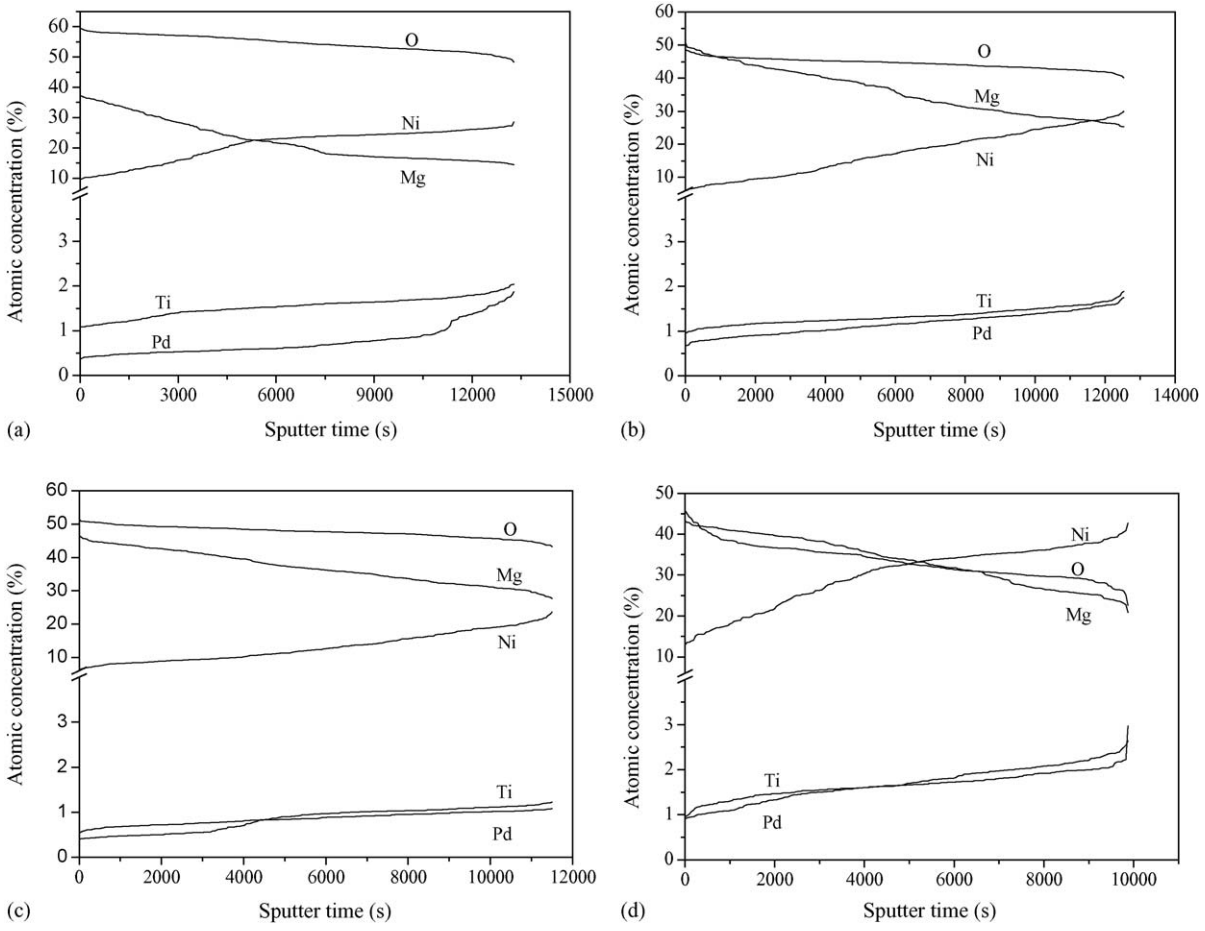

Fig. 7. The AES depth profile of the $Mg_{0.9-x}Ti_{0.1}Pd_xNi$ ($x = 0.04$–0.1) electrode alloys after 40 charge–discharge cycles: (a) $Mg_{0.86}Ti_{0.1}Pd_{0.04}Ni$; (b) $Mg_{0.84}Ti_{0.1}Pd_{0.06}Ni$; (c) $Mg_{0.82}Ti_{0.1}Pd_{0.08}Ni$; (d) $Mg_{0.8}Ti_{0.1}Pd_{0.1}Ni$.

$Mg_{0.86}Ti_{0.1}Pd_{0.04}Ni$ alloy. This can be deduced that the substitution of Pd for Mg effectively inhibited oxidative corrosion on the surface of the $Mg_{0.9-x}Ti_{0.1}Pd_xNi$ ($x = 0.04$–0.1) electrode alloys. The higher Pd amount contained in the alloy, the more significant is the corrosion inhibition effect on the alloy surface. The segregation phenomena of Mg and Ni on the alloys surface as reported by Zhang et al. [20] were also observed in this study. The content distributions of Ti and Pd on the surface were nearly the same for all of the studied electrode alloys.

3.4. Electrode kinetics parameters of the quaternary alloys

Fig. 8 illustrates the electrochemical impedance spectroscopy of the $Mg_{0.9-x}Ti_{0.1}Pd_xNi$ ($x = 0.04$–0.1) electrodes alloy at 50% DOD and 303 K. All the EIS spectra of these electrode alloys consisted of a smaller semicircle in the high-frequency region and a larger semicircle in the low-frequency region followed by a straight line. The EIS data were analyzed using an equivalent circuit as that proposed by Kuriyama et al. [21] (see the inset in Fig. 8). The capacitive components labeled by C are modeled as constant-phase elements (CPE) to describe the depressed nature of the semicircles. R_{el} is ascribed to the electrolyte resistance between the MH electrode and the reference electrode. The semicircle in the high-frequency region, modeled by R_{cp} and C_{cp}, results from the contact resistance between the alloy particles and the current collector. The contact resistance and capacitance between the alloy particles generate the parameters R_{pp} and C_{pp}, respectively. R_{ct} and C_{ct}, representing the semicircle in the low-frequency region, contribute to the charge-transfer reaction resistance and the double-layer capacitance, respectively. R_w is the Warburg impedance.

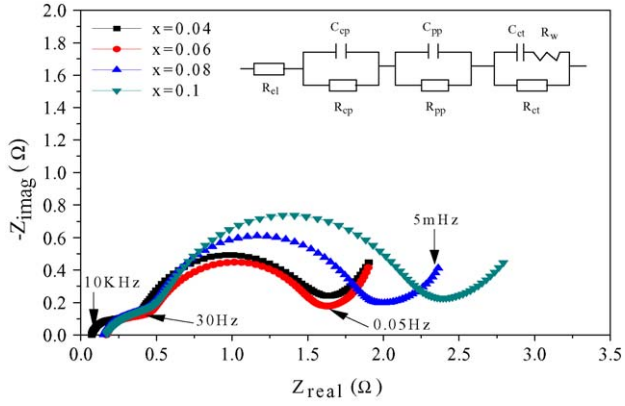

Fig. 8. The electrochemical impedance spectroscopy (EIS) of the $Mg_{0.9-x}Ti_{0.1}Pd_xNi$ ($x = 0.04$–0.1) electrode alloys at 50% DOD and 303 K.

Table 2
Some process kinetics parameters of the $Mg_{0.9-x}Ti_{0.1}Pd_xNi$ ($x = 0.04$–0.1) electrode alloys

x	Charge-transfer reaction resistance, R_{ct} (mΩ)	Polarization resistance, R_p (mΩ)	Exchange current density, I_0 (mA g^{-1})	Limiting current density, I_L (mA g^{-1})	Hydrogen diffusion coefficient, D ($\times 10^{-9}$ cm^2 s^{-1})
0.04	167	1978	256	916	3.0
0.06	223	2100	247	1063	4.1
0.08	250	2382	212	1096	4.9
0.1	273	2892	184	1129	5.6

The parameters in the equivalent circuit were calculated by a complex non-linear least squares fit program of IM6e workstation. The charge-transfer reaction resistance R_{ct} of the electrode alloys was summarized in Table 2. It can be seen that the R_{ct} values increased monotonously from 167 ($x = 0.04$) to 273 mΩ ($x = 0.1$) with increasing Pd content. Previous work [22] also found that additional Pd enhanced the reaction resistance on the surface of Mg-based amorphous alloys. Therefore, the substitution of Pd for Mg caused the retardance of charge-transfer on the surface of the quaternary electrode alloys in the present work.

Fig. 9 shows the linear polarization curves (LP) of the $Mg_{0.9-x}Ti_{0.1}Pd_xNi$ ($x = 0.04$–0.1) electrode alloys at 50% DOD and 303 K. There is a good linear dependence between the current and overpotential within a small overpotential range (±5 mV). The slope of the linear polarization curve corresponds to the polarization resistance R_p of the electrode alloys. In Table 2, it was found that with the increase of Pd content, the R_p values of the electrode alloys increased monotonously from 1978 ($x = 0.04$) to 2892 mΩ ($x = 0.1$). This indicated that the reaction rate was slowed down due to the growth of the passive film on the surface of alloy particles. From Table 2, one can also observe that the variation of R_p values obtained from the linear polarization are consistent with that of R_{ct} values but the former is larger than the latter. In this study, we suggested that the polarization resistance R_p consists of the electrolyte resistance R_{el}, the contact resistance R_{cp} and R_{pp}, and the charge-transfer reaction resistance R_{ct}. The exchange current density I_0 can be calculated by the following formula [23]:

$$I_0 = RT/FR_p \quad (1)$$

where R is the gas constant, T is the absolute temperature, F is the Faraday constant, and R_p is the polarization resistance. The I_0 values of the $Mg_{0.9-x}Ti_{0.1}Pd_xNi$ ($x = 0.04$–0.1) electrode alloys at 50% DOD and 303 K obtained from Eq. (1) were also tabulated in Table 2. It can be seen that the I_0 values of the electrode alloys decreased from 256 ($x = 0.04$) to 184 mA g^{-1} ($x = 0.1$) with the increase of Pd content. The dependency of I_0 upon Pd content was reversible with that of R_p. The decrease of I_0 was also due to the growth of thick passive film, which retarded the charge-transfer on the surface of alloy particle.

3.5. Hydrogen diffusion behavior

Fig. 10 shows the anodic polarization curves of the $Mg_{0.9-x}Ti_{0.1}Pd_xNi$ ($x = 0.04$–0.1) electrode alloys at 50% DOD and 303 K. The limiting current density I_L obtained from the figure represents the hydrogen diffusion kinetics when hydrogen diffusion became the rate control step in the large overpotential region. In this study, it was found that the I_L values of the electrode alloys increased with Pd content (see Table 2). When $x = 0.1$, the I_L exhibits the maximum value (1129 mA g^{-1}). It can be believed that the larger the I_L value, the faster is the dif-

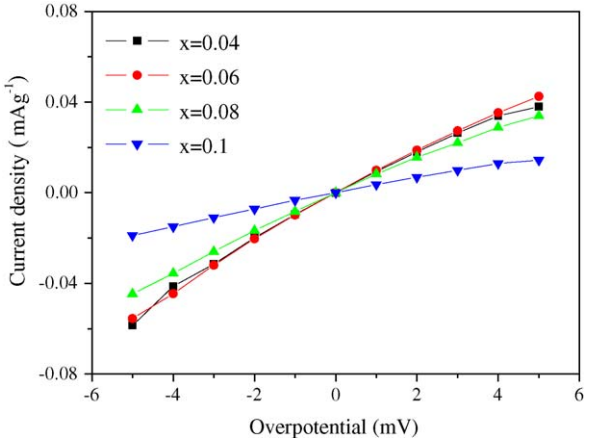

Fig. 9. Linear polarization curves of the $Mg_{0.9-x}Ti_{0.1}Pd_xNi$ ($x = 0.04$–0.1) electrode alloys at 50% DOD and 303 K.

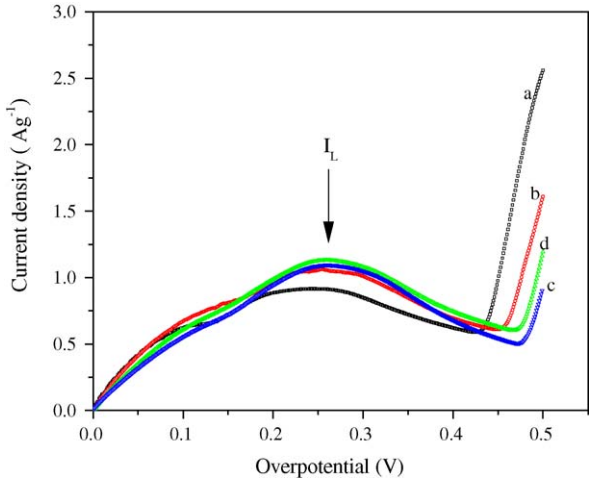

Fig. 10. Anodic polarization curves of the $Mg_{0.9-x}Ti_{0.1}Pd_xNi$ ($x = 0.04$–0.1) electrode alloys at 50% DOD and 303 K: (a) $x = 0.04$; (b) $x = 0.06$; (c) $x = 0.08$; (d) $x = 0.1$.

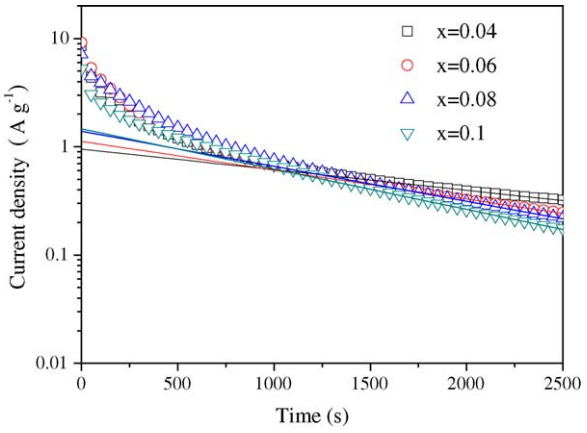

Fig. 11. Semilogarithmic curves of anodic current vs. time response of the $Mg_{0.9-x}Ti_{0.1}Pd_xNi$ ($x=0.04$–0.1) electrode alloys at fully charged state.

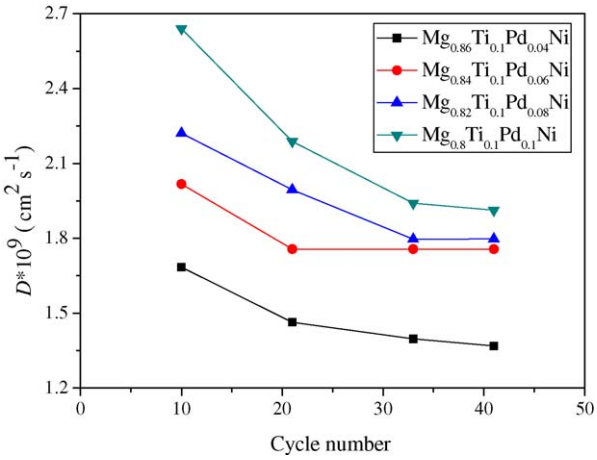

Fig. 12. The variation of hydrogen diffusion coefficient D vs. cycle number for the $Mg_{0.9-x}Ti_{0.1}Pd_xNi$ ($x=0.04$–0.1) electrode alloys during charge–discharge cycles.

fusion of the hydrogen atoms in the alloys [24]. The variation of the I_L values indicated that the hydrogen diffusivity in the alloys increases with Pd content.

In this work, the hydrogen diffusion coefficient D in the bulk of the alloy was estimated by the potential-step method as reported by Ura et al. [25]. Fig. 11 illustrates the semilogarithmic curves of the current–time response of the $Mg_{0.9-x}Ti_{0.1}Pd_xNi$ ($x=0.04$–0.1) electrode alloys at fully charged state. It was found that the value of $\log i$ decreased drastically during the initial time, which means that the concentration of the hydrogen absorbed on the electrode surface became decreasing due to the electro-oxidation. Thereafter, the curve became linear because the rate-determining step changed from electro-oxidation to hydrogen diffusion in the alloy. By fitting the linear section of the current–time response curves as shown in Fig. 11, the hydrogen diffusion coefficient D of the electrode alloys can be calculated according to the following equation [26]:

$$\log i = \log[(6FD/da^2)(C_0 - C_s)] - (\pi^2/2.303)(D/a^2)t \quad (2)$$

in which i, D, C_0, C_s, a, d, and t are the diffusion current density (A g^{-1}), the hydrogen diffusion coefficient ($cm^2\ s^{-1}$), initial hydrogen concentration in the bulk of the alloy (mol cm^{-3}), hydrogen concentration on the surface of the alloy particles (mol cm^{-3}), alloy particle radius (cm), density of the hydrogen storage alloy (g cm^{-3}), and the discharge time (s), respectively. In this work, we supposed the particle average radius was 50 μm after sieving. In Table 2, the calculated D values by Eq. (2) are found increasing from 3.0×10^{-9} ($x=0.04$) to 5.6×10^{-9} $cm^2\ s^{-1}$ ($x=0.1$) with the augment of Pd addition. The hydrogen diffusion coefficient is higher for Pd as compared with other hydrogen storage alloys, such as $LaNi_5$ alloy [25]. Furthermore, the hydrogen diffusivity of crystalline alloys is usually higher than that of amorphous alloys because amorphous alloys do not possess certain channels such as grain boundaries or interfaces for rapid hydrogen diffusion [27]. In the present work, metallic Pd in the amorphous alloys can be regarded as certain convenient channel for hydrogen transferring. The variation of the D values with Pd content in the alloys demonstrated that the hydrogen diffusivity in the alloys was accelerated with the increase of Pd content.

However, with the proceeding of the charge–discharge cycles, the hydrogen diffusion coefficient D decreased gradually as seen in Fig. 12. It can be ascribed to the formation of passive film containing porous $Mg(OH)_2$ and other oxides during the cycle, which retarded the hydrogen diffusion through the surface of electrode alloys. The growth of oxides made it much more difficult for the hydrogen atoms transferring through the passive film. The decrease of diffusivity with cycles may also be due to the oxidation of Pd during the cycles as observed in XPS, the convenient diffusion channels decreased accordingly.

4. Conclusions

The Pd substitution for Mg in $Mg_{0.9-x}Ti_{0.1}Pd_xNi$ ($x=0.04$–0.1) electrode alloys significantly improved the cyclic stability of the electrode alloys. $Mg_{0.8}Ti_{0.1}Pd_{0.1}Ni$ alloy was found possessing the longest cycle life (80 charge–discharge cycles, above 200 mAh g^{-1}). It was demonstrated that Pd played an important role in inhibiting the corrosion of the studied alloys in 6 M KOH solution. XPS and AES measurements found that the introduction of Pd decreased the degree of oxidation of the alloys. The higher the Pd content, the lower is the degree of oxidation. The passive film content was determined as $(NiO)_x(PdO)_y(TiO_2)_z$ oxide composite according to the detection of XPS. The Pd addition also enhanced the corrosion resistance and retarded the charge-transfer in the present study due to the passive film on the alloy surface.

The substitution of Pd for Mg improved the hydrogen diffusivity in the bulk of alloy particles. The limiting current density I_L and the diffusion coefficient D of hydrogen in the alloys increased with the augmentation of Pd content. The hydrogen diffusion coefficient decreased gradually with the proceeding of charge–discharge cycles.

Acknowledgements

The authors wish to express their gratitude and appreciation for the financial support from the National Natural Science Foundation of China (no. 20473091).

References

[1] Y.Q. Lei, Y.M. Wu, Q.M. Yang, J. Wu, Q.D. Wang, Z. Phys. Chem. Bd. 183 (1994) 379–384.
[2] S. Nohara, K. Hamasaki, S.G. Zhang, H. Inoue, C. Iwakura, J. Alloys Compd. 280 (1998) 104–106.
[3] W.H. Liu, H.Q. Wu, Y.Q. Lei, Q.D. Wang, J. Wu, J. Alloys Compd. 261 (1997) 289–294.
[4] H. Ye, Y.Q. Lei, L.S. Chen, H. Zhang, J. Alloys Compd. 311 (2000) 194–199.
[5] S.C. Han, P.S. Lee, J.Y. Lee, A. Züttel, L. Schlapbach, J. Alloys Compd. 306 (2000) 219–226.
[6] Y. Zhang, S.K. Zhang, L.X. Chen, Y.Q. Lei, Q.D. Wang, Int. J. Hydrogen Energy 26 (2001) 801–806.
[7] S. Ruggeri, L. Roué, J. Huot, R. Schulz, L. Aymard, J.M. Tarascon, J. Power Sources 112 (2002) 547–556.
[8] C.S. Wang, Y.Q. Lei, Q.D. Wang, J. Power Sources 70 (1998) 222–227.
[9] T. Kohno, M. Yamamoto, M. Kanda, J. Alloys Compd. 293–295 (1999) 643–647.
[10] S.I. Yamaura, H.Y. Kim, H. Kimura, A. Inoue, Y. Arata, J. Alloys Compd. 347 (2002) 239–243.
[11] T.J. Ma, Y. Hatano, T. Abe, K. Watanabe, J. Alloys Compd. 372 (2004) 251–258.
[12] T.J. Ma, Y. Hatano, T. Abe, K. Watanabe, J. Alloys Compd. 391 (2005) 313–317.
[13] H.J. Park, N.H. Goo, K.S. Lee, J. Electrochem. Soc. 150 (2003) A1328–A1332.
[14] S.I. Yamaura, H.Y. Kim, H. Kimura, A. Inoue, Y. Arata, J. Alloys Compd. 339 (2002) 230–235.
[15] S.I. Yamaura, H. Kimura, A. Inoue, J. Alloys Compd. 358 (2003) 173–176.
[16] Qi-Feng Tian, Yao Zhang, Hai-Liang Chu, Li-Xian Sun, Fen Xu, Zhi-Cheng Tan, Hua-Tang Yuan, Tao Zhang, Abstracts of the 3rd International Conference On Materials for Advanced Technologies (ICMAT 2005) and 9th International Conference On Advanced Materials (ICAM 2005). J. Power Sources, in press.
[17] Y. Zhang, Y.Q. Lei, L.X. Chen, J. Yuan, Z.H. Zhang, Q.D. Wang, J. Alloys Compd. 337 (2002) 296–302.
[18] Y. Zhang, B. Liao, L.X. Chen, Y.Q. Lei, Q.D. Wang, J. Alloys Compd. 327 (2001) 195–200.
[19] W.A. Badawy, K.M. Ismail, A.M. Fathi, Electrochim. Acta 50 (2005) 3603–3608.
[20] Y. Zhang, L.X. Chen, Y.Q. Lei, Q.D. Wang, Electrochim. Acta 47 (2002) 1739–1746.
[21] N. Kuriyama, T. Sakai, H. Miyamura, I. Uehara, H. Ishikawa, T. Iwasaki, J. Alloys Compd. 202 (1993) 183–197.
[22] S. Nakano, S. Yamaura, S. Uchinashi, H. Kimura, A. Inoue, Mater. Trans. 45 (2004) 1367–1370.
[23] P.H.L. Notten, P. Hokkeling, J. Electrochem. Soc. 138 (1991) 1877–1885.
[24] B.V. Ratnakumar, C. Witham, R.C. Bowman Jr., A. Hightower, B. Fultz, J. Electrochem. Soc. 143 (1996) 2578–2584.
[25] H. Ura, T. Nishina, I. Uchida, J. Electroanal. Chem. 396 (1995) 169–173.
[26] G. Zhang, B.N. Popov, R.E. White, J. Electrochem. Soc. 142 (1995) 2695–2698.
[27] Ming Au, Mater. Sci. Eng. B 117 (2005) 37–44.